Nucleic Acids Research, 2006, Vol. 34, No. 5 ***1305–1316***
doi:10.1093/nar/gkl004

Inhibitory effects of archetypical nucleic acid ligands on the interactions of HIV-1 nucleocapsid protein with elements of Ψ-RNA

Kevin B. Turner, Nathan A. Hagan and Daniele Fabris*

Department of Chemistry and Biochemistry, University of Maryland Baltimore County, 1000 Hilltop Circle, Baltimore, MD 21228 USA

Received January 24, 2006; Revised and Accepted February 10, 2006

ABSTRACT

Disrupting the interactions between human immunodeficiency virus type 1 (HIV-1) nucleocapsid (NC) protein and structural elements of the packaging signal (Ψ-RNA) could constitute an ideal strategy to inhibit the functions of this region of the genome leader in the virus life cycle. We have employed electrospray ionization (ESI) Fourier transform mass spectrometry (FTMS) to assess the ability of a series of nucleic acid ligands to bind selected structures of Ψ-RNA and inhibit their specific interactions with NC *in vitro*. We found that the majority of the ligands included in the study were able to form stable non-covalent complexes with stem–loop 2, 3 and 4 (SL2–4), consistent with their characteristic nucleic acid binding modes. However, only aminoglycosidic antibiotics were capable of dissociating preformed NC•SL3 and NC•SL4 complexes, but not NC•SL2. The apparent specificity of these inhibitory effects is closely dependent on distinctive structural features of the different NC•RNA complexes. The trends observed for the IC_{50} values correlate very well with those provided by the ligand binding affinities and the dissociation constants of target NC•RNA complexes. This systematic investigation of archetypical nucleic acid ligands provides a valid framework to support the design of novel ligand inhibitors for HIV-1 treatment.

INTRODUCTION

A primary cause of failure of the highly active anti-retroviral therapy (HAART) used to control the infection of human immunodeficiency virus type 1 (HIV-1) is the rapid emergence of strains that are resistant to one or more of the active agents used in typical multidrug regimens (1,2). Mutations of genes coding for inhibitor targets, such as protease, reverse transcriptase and gp41, result in a reduced response to treatment from patients infected by resistant strains (3–5). The magnitude reached by the AIDS pandemic and the daunting problem of drug resistance elevate the need for new therapeutic agents with alternative mechanisms of action (6–8).

In the life cycle of HIV-1, the processes of genome recognition, dimerization and packaging provide very attractive opportunities for the development of novel anti-retroviral strategies. These essential functions are mediated by the interactions between the nucleocapsid (NC) domain of the *Gag* polyprotein (9,10) and a highly conserved region of genomic RNA, known as the packaging signal, or Ψ-RNA (11–13). The structure of NC includes two zinc-finger motifs of retroviral type (CCHC, Figure 1) (14,15), which are responsible for its activity as a nucleic acid chaperone (16). Located in the 5′-untranslated region (5′-UTR), the ∼120 nt comprising Ψ-RNA have been shown to fold into relatively stable secondary structures identified as stem–loop 1 through 4 (SL1–4), which serve as possible binding sites for NC during viral replication (17–19). The characteristics and structural determinants of these protein–RNA interactions have been extensively investigated to elucidate the role played by the different elements [reviewed in ref. (20)] and enable the identification of viable targets.

Different strategies have been proposed to disrupt the mechanism of genome recognition, dimerization and packaging by targeting key structures involved in these processes. Based on the observation that intact zinc-fingers are crucial for NC activity, different chemical agents have been investigated for their ability to induce Zn^{2+} ejection and protein deactivation (21–23). Peptides mimicking the 3D structure of NC, which are intended to compete with the protein for its recognition sites on genomic RNA, were either synthesized (24), or isolated from phage-displayed libraries (25,26). Antisense oligonucleotides were designed to hybridize with the palindromic sequence of SL1 (27,28) and inhibit the inter-strand base pairing that initiates genome dimerization (29–31).

*To whom correspondence should be addressed. Tel: +1 410 455 3053; Fax: +1 410 455 2608; Email: fabris@umbc.edu

© The Author 2006. Published by Oxford University Press. All rights reserved.

The online version of this article has been published under an open access model. Users are entitled to use, reproduce, disseminate, or display the open access version of this article for non-commercial purposes provided that: the original authorship is properly and fully attributed; the Journal and Oxford University Press are attributed as the original place of publication with the correct citation details given; if an article is subsequently reproduced or disseminated not in its entirety but only in part or as a derivative work this must be clearly indicated. For commercial re-use, please contact journals.permissions@oxfordjournals.org

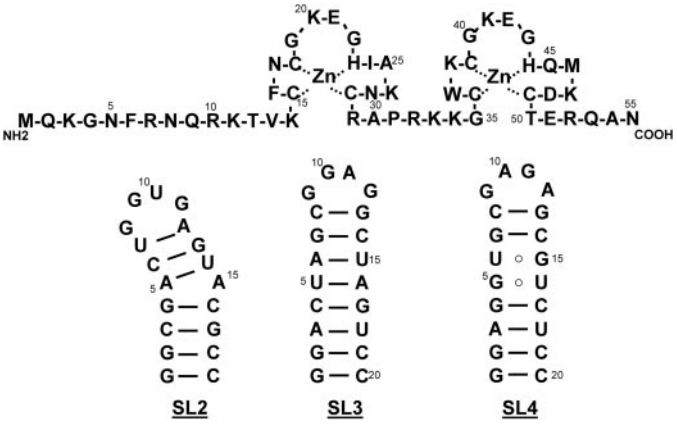

Figure 1. Sequence of the NC domain of the *Gag* polyprotein and secondary structures of individual stem–loops (SL2–4) of the HIV-1 packaging signal.

Efforts aimed at finding small ligands that interfere with the packaging signal have revealed the ability of aminoglycoside analogues to bind specific structures of Ψ-RNA *in vitro* (32–35). The primary binding site was identified near the dimerization initiation site on SL1, which is consistent with the striking structural similarities between the dimeric form of this stem–loop and the ribosomal aminoacyl-tRNA site (A-site) of prokaryotes (34). However, depending on the subtype sequence and experimental conditions employed for the assays, binding was observed for both monomeric (32,33) and dimeric forms of SL1 (34), thus casting doubt on the ability of aminoglycosides to inhibit RNA dimerization.

In this report, we examine the interactions of a selection of small molecule ligands with separate domains of the packaging signal and their complexes with NC. Representative members of different classes of nucleic acid binders (36–38) were selected to sample archetypical structures that may constitute valid templates for the development of new anti-retroviral agents. Substrates included in the study consist of RNA hairpins SL2 and SL3 (Figure 1), which are not believed to be directly involved in genome dimerization, but provide specific binding sites for NC during genome recognition and packaging (17,18,20). In addition, a construct corresponding to the putative SL4 has been investigated to gain further insights into the mechanism of inhibition of NC–RNA interactions *in vitro*, even though the possible participation of this sequence in long-range base pairing interactions casts doubt on the actual existence of a discrete stem–loop structure *in vivo* (39) and in full-length 5′-UTR constructs *in vitro* (40,41). An approach based on electrospray ionization (ESI) (42,43) and Fourier transform mass spectrometry (FTMS) (44,45) was followed to investigate ligand–RNA interactions and evaluate the stability of NC-hairpin complexes in the presence of ligands. The inherent low energy involved with this ionization technique enables the observation of labile non-covalent complexes, which remain intact in the gas-phase (46–48). This characteristic has led to the successful investigation of protein–nucleic acid, nucleic acid–nucleic acid and small ligand–nucleic acid interactions by mass spectrometry [reviewed in ref. (49,50)]. In a recent study, we employed ESI-FTMS to determine the stoichiometry and binding affinity of NC for SL2, SL3 and SL4 in solution (51). We have now extended this approach to explore possible inhibitory effects on NC-hairpin complexes in solution. The results are discussed in the context of the specific structural features of substrates and ligands, in an effort to understand the binding determinants and the possible implications for the development of new therapeutic strategies aimed at interfering with the interactions of NC with the RNA packaging signal.

MATERIALS AND METHODS

RNA sample preparation

Oligo-ribonucleotides matching the sequences of SL2, SL3 and SL4 from the NL4-3 strain of HIV-1 (Figure 1) were purchased from Dharmacon, Inc. (Lafayette, CO), deprotected according to manufacturer's recommendations, and extensively desalted by ultrafiltration on Centricon YM-3 devices (Millipore, Bedford, MA) using a 100 mM solution of ammonium acetate (pH 7.5). Three additional base pairs were included at the base of the SL4 stem to stabilize its secondary structure. The purity and integrity of each sample were confirmed by ESI-FTMS (see e.g. Figure 3a). The concentration of each stock solution was determined by ultraviolet (UV) absorbance, using the following molar absorptivities: 190.07 $mM^{-1}cm^{-1}$ for SL2, 186.55 $mM^{-1}cm^{-1}$ for SL3, and 201.99 $mM^{-1}cm^{-1}$ for SL4. Immediately prior to use, each construct was heated to 95°C for 3 min and quickly cooled on ice to achieve proper folding of the hairpin structures.

NC sample preparation

An expression vector containing the gene for NC (a gift from M. F. Summers, Howard Hughes Medical Institute, University of Maryland, Baltimore County) was transformed and expressed in *Escherichia coli* BL21(DE3)-pLysE cells. NC was purified under non-denaturing conditions (52) and then desalted by ultrafiltration using 100 mM ammonium acetate (pH 7.5), as described for the RNA samples. The purity and integrity of the protein, including the presence of two coordinated Zn^{2+} ions, were confirmed by ESI-FTMS, while the sample concentration was determined by UV absorbance (6.41 $mM^{-1}cm^{-1}$ molar absorptivity).

Ligand–RNA binding

All ligands used in the study were obtained from Sigma Chemical Co. (St. Louis, MO) and utilized without further purification. Stock solutions were prepared by weighing each compound and dissolving it in 100 mM ammonium acetate (pH 7.5). Solutions containing equimolar concentrations of up to three ligands at a time (120 μM each) were prepared from the initial stocks to perform multiplexed binding assays. For each step of the titration series, aliquots of RNA substrate and multi-ligand solution were mixed together and added with an appropriate volume of 100 mM ammonium acetate (pH 7.5) to obtain a fixed final 0.35 μM concentration of RNA. Total ligand concentrations ranged between 0.35 and 17.5 μM in subsequent steps, corresponding to a 0.1- to 5-fold excess of total ligand. Each sample was incubated at room temperature for 15 min to ensure that a binding equilibrium was established in solution before ESI-FTMS analysis. Control experiments performed with longer incubation provided no detectable

difference in binding. The determination of individual dissociation constants was performed in similar fashion by preparing fixed 0.35 μM solutions of RNA in the presence of 0.35–17.5 μM of each ligand in 100 mM ammonium acetate (pH 7.5). The upper boundary of ligand concentrations was generally set to a 5-fold excess (17.5 μM) over RNA substrate after control experiments on an unstructured oligo-deoxyribonucleotide had shown that a 7-fold excess (24.5 μM) or more of each drug could lead to non-specific aggregation.

NC–RNA inhibition

Complexes of NC with the different stem–loops were obtained by mixing equimolar amounts of each component in 100 mM ammonium acetate (pH 7.5). After 15 min at room temperature, the formation of the desired 1:1 complexes was verified using ESI-FTMS (see e.g. Figure 7a), as described in ref. (51). Inhibition experiments consisted of the addition of increasing amounts of ligand to a fixed concentration of preformed NC-stem–loop complex. In this case, each final solution contained ~3.5 μM of complex (from the initial concentrations of NC and RNA) and 0.35–17.5 μM of inhibitor in 100 mM ammonium acetate (pH 7.5).

Mass spectrometry

Immediately prior to analysis, analyte solutions were mixed with a 10% volume of 2-propanol to reduce the surface tension and facilitate the achievement of stable electrospray (47). This addition did not have any adverse effect on the state of association of the non-covalent complexes investigated in this study (51), but the dilution factor was taken in account in subsequent calculations. Approximately 5 μl of each sample was loaded into a nanospray needle made of uncoated borosilicate. A Pt-wire was inserted from the back to carry the necessary voltage (750–1000 V). Each analysis was performed on a Bruker Daltonics (Billerica, MA) Apex III FTMS system equipped with a 7 T actively shielded superconducting magnet and an Apollo thermally assisted electrospray source. The desolvation interface was set to a temperature of 170°C. Spectra were acquired in negative ion mode and processed using XMASS 6.0.2 (Bruker Daltonics). A resolving power of ~150 000 was typically obtained in broadband mode. An accuracy of ~10 p.p.m. or better was achieved using a three-point external calibration of cesium iodide.

Data analysis

Concentrations of free and bound species obtained upon ligand addition were calculated from the known initial concentrations of RNA or NC–RNA complex by using the molar fractions of the different species in solution, which was directly determined from the intensity of the respective signals divided by their charge state (51,53). This method relies on the reasonable assumption that any effect induced upon binding of a small ligand to a much larger and highly charged substrate is likely to result in a minor shift of the overall charge state distribution, rather than in complete signal suppression. Therefore, using all the signals detected for each species divided by their charge state can account for such a shift. In our case, the validity of such assumption was confirmed by the fact that no significant changes of charge distribution could be detected during the binding experiments (see Results and Discussion).

Solution concentrations obtained from the respective molar fractions were employed to plot binding curves and calculate the respective dissociation constant (K_d) using the data-fitting algorithm included in Origin 7 (Silverdale Scientific, Buckinghampshire, UK). All titration experiments were performed at least in triplicate, thus the reported precision reflects the overall uncertainty of each K_d determination.

Considering that each inhibition experiment was limited to a maximum 5-fold ligand addition to avoid non-specific aggregation, the ligand concentration causing 50% dissociation of initial complex (IC_{50}) was obtained from the available data using the isotherm curve that describes the competition of two ligands for the same binding site:

$$\text{fractional occupancy} = \frac{[L]}{K_{comp} + [L]},$$

where the fractional occupancy corresponds to the percent of ligand–RNA complex determined experimentally in the presence of [L] ligand concentration, while K_{comp} represents the apparent dissociation constant of the ligand–RNA complex under competition conditions. After subsequent increases of ligand, the curve fitted by Origin 7 was used to obtain the [L] corresponding to a 0.5 fractional occupancy, or IC_{50}. As indicated for K_d determinations, each experiment was performed in triplicate and Origin 7 was used to calculate the overall precision of each IC_{50} value.

RESULTS AND DISCUSSION

Ligands selected for the study consist of molecules representing widely different structures and binding modes with nucleic acids (Figure 2). Many of these compounds are established agents used in antineoplastic, antibacterial or antiviral therapy (36–38). Grouped according to the general binding mechanism, the library includes intercalators (ethidium bromide, acridines and tetracyclines), minor groove-binders (distamycin A, Hoechst 33258 and 33342), mixed-mode intercalator/minor groove-binders (mitoxantrone, daunomycin, actinomycin D, chromomycin A3), and multifunctional polycationic aminoglycosides (neomycin B, paromomycin and tobramycin). The glycopeptide antibiotic vancomycin was included as a negative control for its known activity toward peptidoglycan units of bacterial cell walls (54,55).

Assessing ligand–RNA interactions

Specific interactions between ligands and hairpin SL2, SL3 and SL4 (Figure 1) were investigated by high-resolution mass spectrometry to obtain the composition and stoichiometry of ligand–RNA complexes in solution. Initially, a multiplexed strategy was implemented to complete a rapid screening of the binding abilities of each ligand. Different ligands were combined in equimolar amounts to enable their simultaneous addition to a fixed amount of RNA sample (see Materials and Methods). Multiplexing promotes competition among ligands for the same substrate and requires sufficient resolution to unambiguously discriminate the different complexes according to their unique molecular masses (56,57).

The principle is clearly illustrated by representative ESI-FTMS spectra recorded upon stepwise additions of a ternary

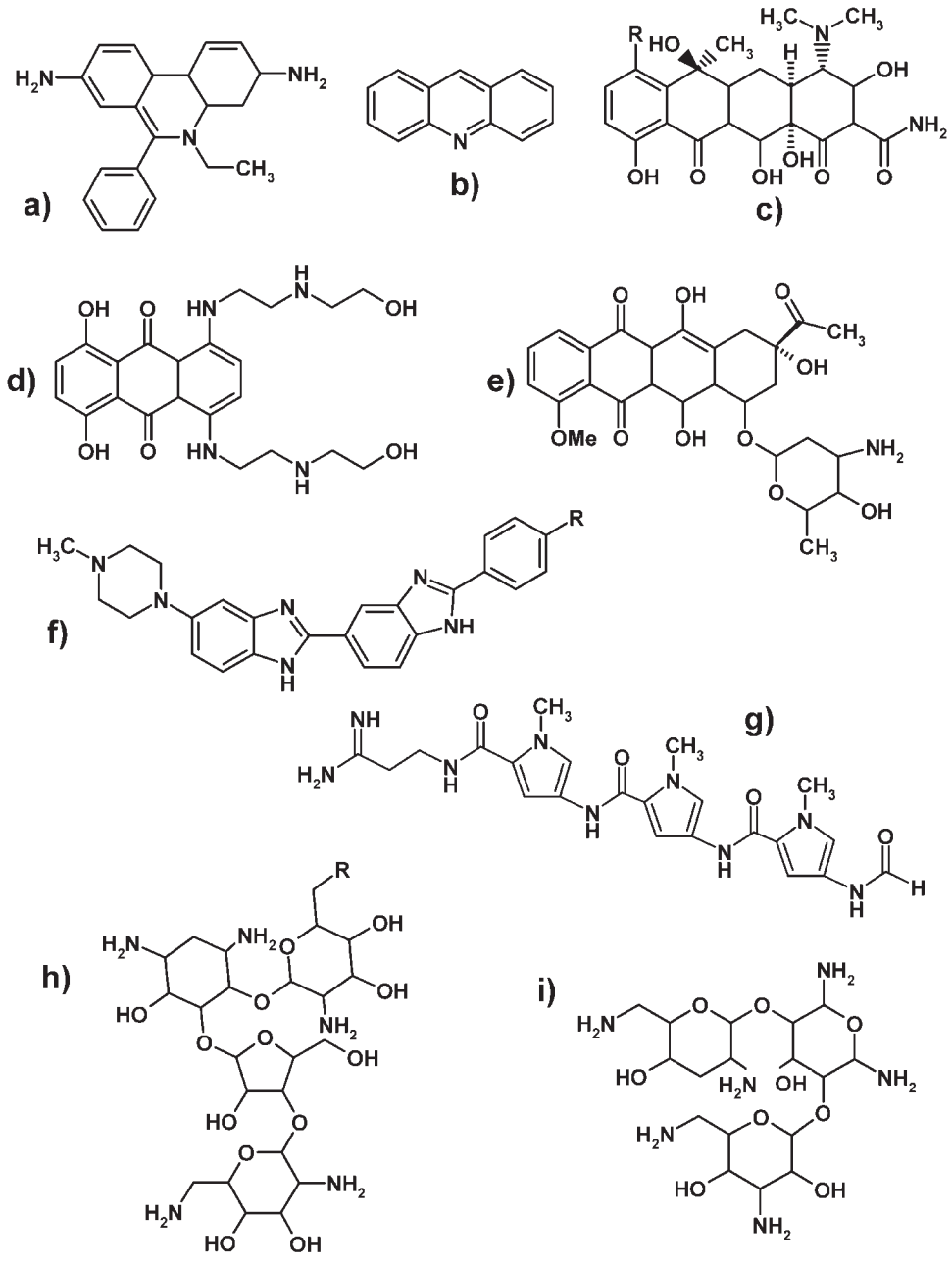

Figure 2. Structures of nucleic acid-active agents incorporated in the study. Intercalators included: (**a**) ethidium bromide; (**b**) acridine; (**c**) tetracycline R = H; chlorotetracycline R = Cl. Mixed-mode binders included: (**d**) mitoxantrone; (**e**) daunomycin. Minor groove-binders included: (**f**) Hoechst33258 R = OH; Hoechst 33342 R = OEt; (**g**) distamycin A. Aminoglycosides included (**h**) neomycin B R = NH_2; paromomycin R = OH; (**i**) tobramycin. Structures not shown but analyzed in the study: vancomycin, actinomycin D and chromomycin A3.

mixture of vancomycin, mitoxantrone and neomycin B to a fixed amount of SL2 (Figure 3, see Materials and Methods). In the region encompassing the four charge state, the signal provided by free SL2 was readily resolved from those corresponding to its 1:1 complexes with mitoxantrone and neomycin B (Figure 3b). The fact that no binding was observed for vancomycin is consistent with its lack of activity towards nucleic acids and excludes the possibility that non-specific aggregation might occur during sample handling or analysis. Further additions of ternary mixture provided concentration-dependent increases of the signals recorded for the neomycin and mitoxantrone complexes (Figure 3c), with concomitant decreases of those corresponding to free RNA substrate. The pattern provided by these experiments is consistent with the following relative scale of binding affinity: neomycin B > mitoxantrone >> vancomycin.

After initial multiplexed screening, the ligands with detectable binding were analyzed individually to determine the dissociation constant (K_d) of their respective RNA complexes (58–60). The fact that no significant changes were noted in the ESI charge states distributions upon binding is a strong indication that the complexes' ionization characteristics are largely determined by the highly charged RNA components. When this condition is verified, the signals corresponding to

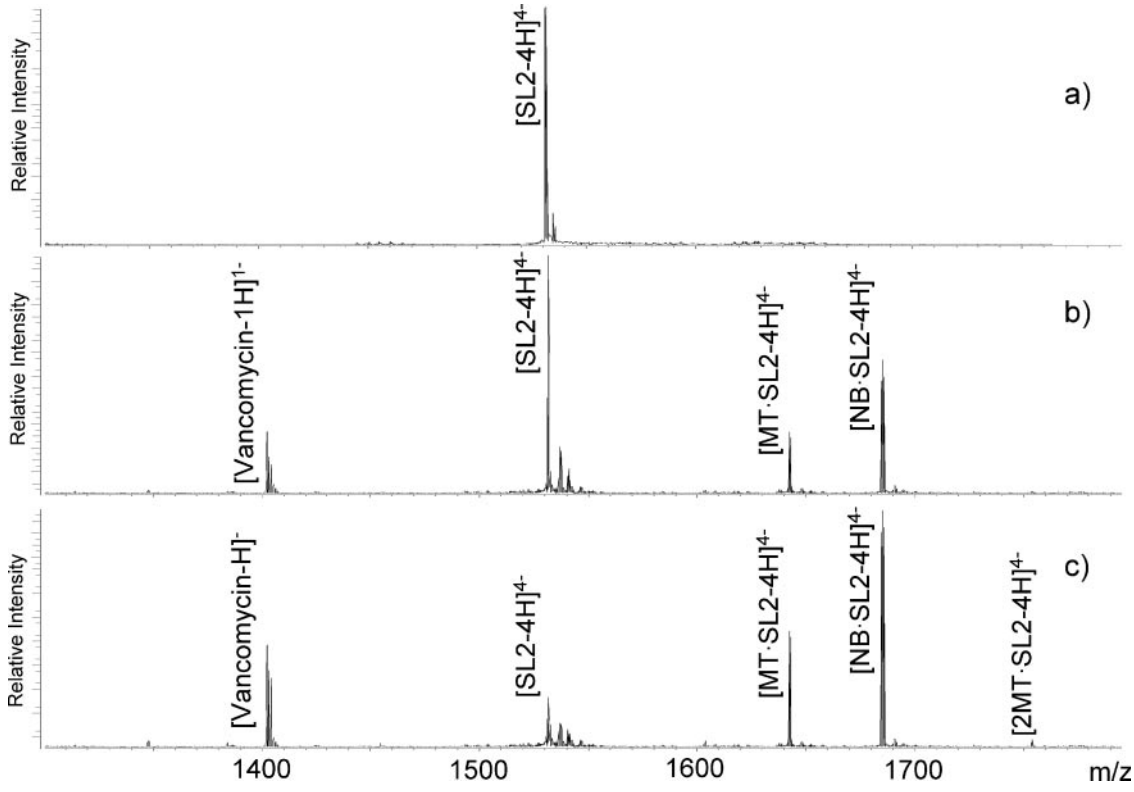

Figure 3. (**a**) ESI-FTMS of 3.5 μM SL2 in 100 mM ammonium acetate (pH 7.5) and 10% volume 2-propanol. In the absence of ligand, SL2 provided an experimental mass of 6128.89 Da (6128.86 Da calculated from sequence). (**b**) ESI-FTMS of 3.5 μM SL2 in the presence of 1-fold equimolar mixture of mitoxantrone (MT), neomycin B (NB) and vancomycin (see Materials and Methods). The 1:1 complex MT•SL2 provided a mass of 6573.11 Da (6573.06 Da calculated), while NB•SL2 provided 6473.20 Da (6473.17 Da calculated). Unbound vancomycin was observed with a mass of 1407.45 Da (1407.43 Da calculated). (**c**) 3.5 μM SL2 with 5-fold equimolar mixture of MT, NB and vancomycin. Higher order stoichiometries were observed for MT (e.g. 2MT•SL2), resulting in increments of 444.20 Da.

free and bound stem–loops can be used to calculate the corresponding molar fractions, which in turn can provide their respective concentrations in solution (see Materials and Methods) (51). The titration of each RNA substrate with individual ligands provided characteristics binding curves exemplified in Figure 4 (see also Supplementary Data).

The K_d values obtained for the 1:1 ligand–RNA complexes analyzed in our study are summarized in Table 1. The individual ligands were analyzed in separate titrations to ensure the best possible accuracy for this type of quantitative determination and to safeguard against undesirable ligand–ligand interactions. The initial multiplexed screening reported very weak binding interactions for actinomycin D, which was detected only at the highest ligand concentrations (61). Similar results were provided by chromomycin A3, even in the presence of Zn^{2+} in a 2:1 drug to metal ratio, which is known to stabilize its biding to double-stranded oligodeoxyribonucleotides (62). For this reason, individual K_d's were not determined for these two ligands.

Binding modes to Ψ-RNA stem–loops

The target RNA constructs used in our study share a common hairpin structure including a double-stranded stem stabilized by GC base pairs and a flexible single-stranded loop formed by four unpaired nucleotides (Figure 1). However, only SL3 presents a regular A-type helical stem (60), which enables the observation of baseline ligand activity in the absence of more complex structural features.

The results provided by SL3 are consistent with the characteristic binding modes of the classes of nucleic acid-active molecules included in the study. For example, the intercalators ethidium bromide and acridine provided the lowest K_d's in the library, which can be explained by the strong stacking interactions between their planar aromatic systems and the GC pairs of the stem region (63,64). Consistent with the presence of multiple putative sites, complexes including up to a maximum of three equivalents were observed. Although tetracyclines have been suggested to bind the hammerhead ribozyme through an intercalating mechanism (65), only one of their rings is actually aromatic (Figure 2) and the fused system is not completely planar. Therefore, reduced van der Waals stabilization is likely the cause of the low binding affinity shown by chlorotetracycline, which was the weakest ligand in the library (Table 1).

The complexes of the antineoplastic drug mitoxantrone (Figure 2) with B-type DNA are stabilized by a combination of intercalation and polar interactions between its side chains and the functional groups exposed on the minor groove surface (66). However, SL3 presents a typical A-RNA minor groove, which is much wider and shallower. The spacing between polar groups does not appear to favor the side chain interactions that provide additional stabilization to mitoxantrone binding. The very weak affinity manifested by other

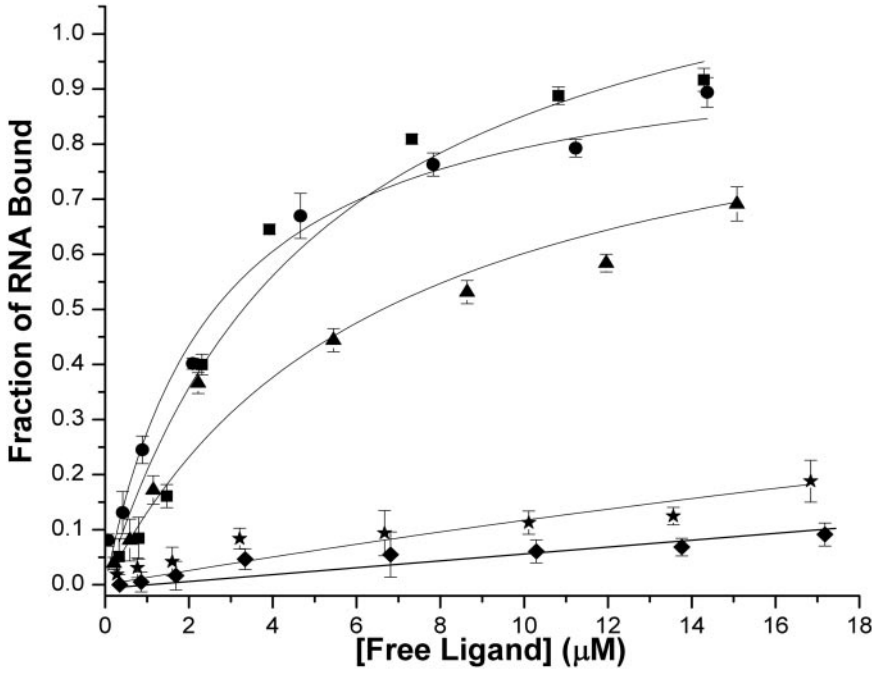

Figure 4. Ligand–SL2 binding curves. For the sake of clarity, only one representative curve is shown for each class of ligands: neomycin B (filled square), ethidium bromide (filled circle), mitoxantrone (filled triangle), distamycin A (filled star) and chlorotetracycline (filled diamond). See Materials and Methods for conditions. See Supplementary Data for ligand–SL3 and ligand–SL4 binding curves.

Table 1. Summary of dissociation constants (K_d's) determined for stem–loop complexes with individual ligands

Ligand	SL2	SL3	SL4
Neomycin B	3.0 ± 0.6	4.2 ± 0.3	1.0 ± 0.2
Paromomycin	8.8 ± 1.1	37.7 ± 1.3	8.0 ± 1.1
Tobramycin	9.7 ± 1.6	38.7 ± 3.7	7.8 ± 1.1
Ethidium Bromide	2.6 ± 0.2	1.9 ± 0.2	12.7 ± 1.6
Acridine	2.8 ± 0.3	2.4 ± 0.3	12.7 ± 1.4
Mitoxantrone	6.6 ± 0.7	3.9 ± 0.5	10.0 ± 0.7
Daunomycin	22.7 ± 3.6	8.2 ± 0.9	12.1 ± 0.9
Distamycin A	75.4 ± 7.5	28.5 ± 4.7	57.9 ± 3.5
Hoechst 33342	99.9 ± 12.5	88.2 ± 6.6	170.6 ± 17.9
Chlorotetracycline	161.1 ± 14.8	883.5 ± 299.6	391.0 ± 81.1

All values of K_d are expressed in μM units. In preliminary multiplexed screening, Hoechst 33258 and tetracycline displayed very similar binding activities to Hoechst 33342 and chlorotetracycline, respectively, thus these ligands were not subjected to individual titrations.

intercalator/groove-binders with larger side chains of peptidic (i.e. actinomycin D) (67,68) or carbohydrate nature (i.e. chromomycin A3) (69,70) suggests a similar mismatch with the position of suitable functional groups on the RNA surface. The wider and shallower minor groove of A-RNA is also at the basis of the limited stabilization received by the minor groove-binders distamycin A and Hoechst 33258/33342 (Figure 2) (71,72). The higher affinity shown by the former is consistent with a stronger electrostatic contribution from its basic amidino-group (73).

Among the aminoglycoside antibiotics, neomycin B exhibited the highest affinity toward SL3, with a K_d slightly higher than generic intercalators and similar to mitoxantrone (Table 1). Paromomycin and tobramycin provided higher K_d values, which are within range of the minor groove-binder distamycin A. This group of drugs relies on a flexible scaffold to adapt to complex substrate structures and possesses the ability to form multiple hydrogen bonds and electrostatic interactions with RNA (Figure 2) (34,59,74,75). The overall molecular architecture does not appear to be determinant in modulating the strength of the interaction with SL3-RNA, as suggested by the fact that paromomycin and tobramycin include four and three carbohydrate rings, respectively, but still bind with very similar K_d's. On the contrary, the presence of six amino groups in neomycin B versus five in the other two aminoglycosides can account for the higher affinity shown by the former. This observation is consistent with a significant electrostatic component in the binding mechanism, which involves strong interactions between protonated amino groups and negative regions of the RNA substrate.

RNA structural determinants of binding activity

The Ψ-RNA stem–loops possess very distinctive structural features that are expected to profoundly modify the binding modes manifested by small ligands. Each single-stranded loop presents a different base composition and can assume variably flexible conformations stabilized by limited stacking and hydrogen bonds (76–78). This flexibility facilitates protein binding and possibly RNA–RNA tertiary interactions with other regions of the 5′-UTR. However, in the context of isolated hairpin constructs, this characteristic does not facilitate the formation of well-defined sites or stable pockets for the specific binding of small ligands. On the contrary, the double-stranded stems present relatively stable motifs that could serve as potential binding sites. In particular, the AUA triple base platform of SL2 and the tandem GU wobbles of SL4 provide far greater opportunities for specific interactions than the SL3's uninterrupted helical structure.

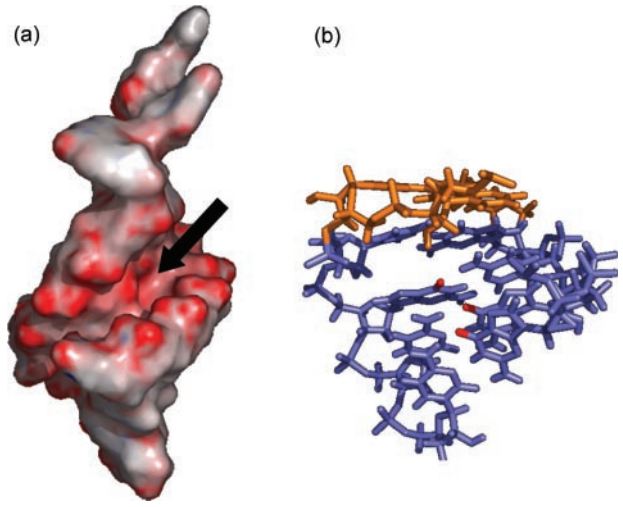

Figure 5. (**a**) SL2 electrostatic surface (PDB:1ESY) calculated for a 100 mM salt environment utilizing Delphi (85) and visualized in Pymol (86). The red coloring marks highly electronegative regions, such as the phosphates and the major groove below the AUA triple base platform. (**b**) The bases forming the AUA platform are colored in orange, while the O6 of G1, G2 and G17 lining the electronegative pocket are highlighted in red.

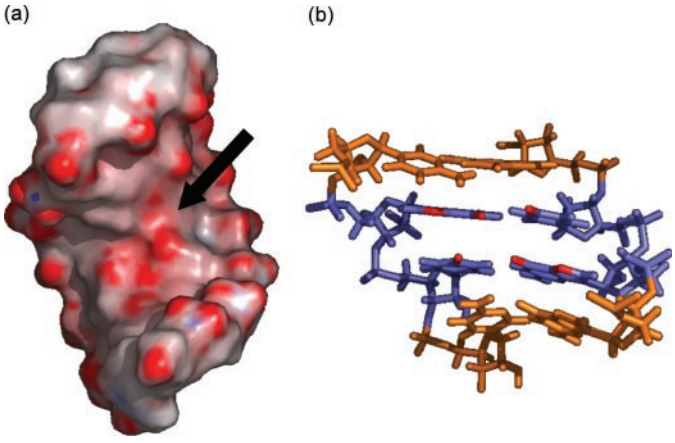

Figure 6. (**a**) SL4 electrostatic surface (PDB: 1JTW) calculated in a 100 mM salt environment utilizing Delphi (85) and visualized in Pymol (86). The red area indicated by the arrow corresponds to a negatively charged surface in the major groove of the tandem GU wobbles. (**b**) Highlighted in red, the N7 and O6 of G5 and G15 form this electronegative region, together with the O4 of U6 and U16. The base pairs flanking the wobbles are colored in orange.

In the case of SL2, base mismatches in the helical region of the stem–loop create a kink that enables the nucleobase of U14 to become approximately co-planar with those of A5 and A15 to complete a triple base structure (78). The platform motif causes a shift of the helical axis in the midsection of the stem and subjects the minor groove to significant opening (Figure 5a). This situation causes subtle changes in the normal base-stacking pattern, which result in a noticeable decrease of affinity for intercalating molecules (Table 1). The dimensions and surface of the minor groove are distorted to a degree that makes this region even less favorable to minor groove-binders. This is consistent with the greatly reduced affinity of distamycin A and Hoechst 33258/33342 toward SL2 than toward SL3. On the contrary, the affinity for SL2 displayed by the aminoglycosides was significantly higher. Considering the electrostatic character of aminoglycoside binding, this increase suggests the possible interaction with a highly negative region created by the close proximity of the O6 of G1, G2 and G17 in the major groove below the AUA platform (Figure 5a and b). Competition experiments aimed at comparing the binding activity of wild-type SL2 with a mutant in which the platform was eliminated by deletion of A15 showed a 50% reduction in aminoglycoside affinities (see Supplementary Data), thus supporting the role played by this structure in ligand binding. Selective gas-phase fragmentation of the neomycin–SL2 complex has recently provided further confirmation of the putative binding site (79).

The structure of SL4 includes contiguous GU pairs (tandem wobbles, Figure 1), which involve non-canonical base pairing interactions. This arrangement forces the double-stranded stem to assume a wider and less compact conformation, which causes a discontinuity in the stacking pattern and reduces its stability to thermal denaturation (77). These effects contribute to the inferior binding of intercalators to this substrate as compared to both SL3 and SL2. The decreased affinity experienced by mitoxantrone was not as prominent because of its preference for GC base pairs (66). This observation points towards sites located away from the tandem wobbles and closer to the loop or the base of the stem (Figure 1). The wider dimensions of the minor groove greatly affected the K_d of groove-binders, but the large electrostatic component in the distamycin mechanism limited its affinity loss (Table 1).

The functional groups exposed on the surface of the tandem wobbles combine to provide an ideal situation for binding the aminoglycosidic antibiotics. In fact, the major groove presents a highly negative region (Figure 6a and b), which is created by placing the G-N7, G-O6 and U-O4 of each wobble on the same plane and in close proximity to each other (80). Delimited by the amino groups of the GC pairs above and below the wobbles, this area constitutes an excellent binding site for positively charged aminoglycosides, which in fact offered the lowest K_d's of the library. This hypothesis was tested using competitive binding experiments that included a mutant SL4m in which G5 and G15 were substituted by A to eliminate the tandem wobbles and obtain a double-stranded stem similar to that of SL3 (see Supplementary Data). The observed SL4 >> SL4m $\approx$ SL3 relative binding scale is consistent with the strong stabilizing effects of the wobble structure on the aminoglycosides interactions. The location of this binding site was further supported by gas-phase fragmentation experiments (79).

Inhibition of NC binding activity

The effects of ligands on the specific binding of NC protein to the Ψ-RNA substrates were investigated *in vitro* by adding increasing amounts of ligand to preformed NC-hairpin complex (see Materials and Methods). Using experimental conditions optimized earlier to determine the stoichiometry and dissociation constants of these protein–RNA assemblies (51), ESI-FTMS was applied to characterize the species present in solution upon addition of ligand and reveal the fate of the protein–RNA complex. As exemplified in Figure 7 and summarized in Table 2, at least three different outcomes were realized: (i) no detectable effects; (ii) dissociation of the protein–RNA complex; (iii) binding of ligand to the

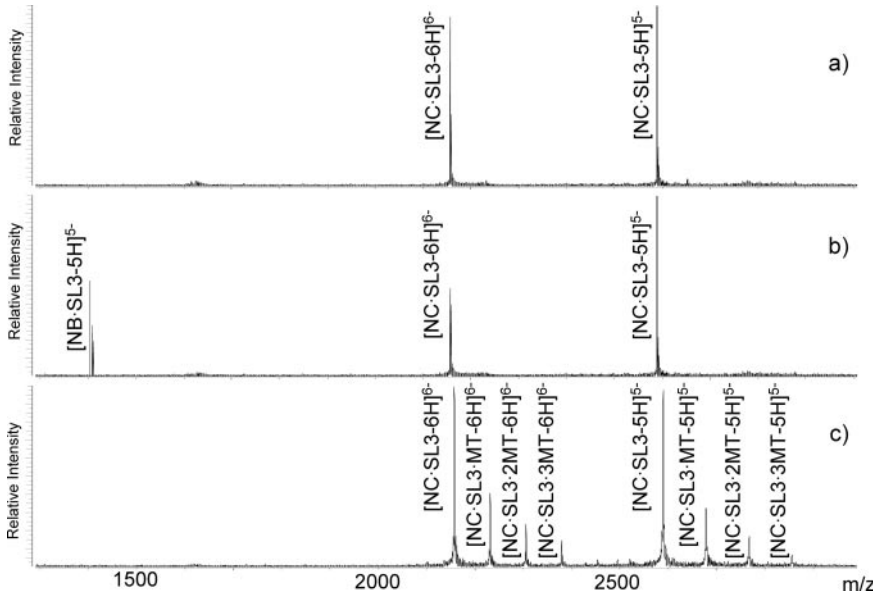

Figure 7. (**a**) ESI-FTMS of 3.5 μM NC•SL3 in 100 mM ammonium acetate (pH 7.5) and 10% volume 2-propanol. In the absence of ligand, NC•SL3 provided an experimental mass of 12 946.90 Da (12 946.94 Da calculated from the respective sequences, including two Zn^{2+} ions). (**b**) 5-fold addition of neomycin B (NB) induced dissociation of NC•SL3 and formation of NB•SL3 with an observed mass of 7072.20 Da (7072.23 Da calculated). (**c**) A ternary species NC•SL3·MT was observed with a mass of 13 391.14 Da (13 391.03 Da calculated) upon 5-fold addition of mitoxantrone (MT) under the same conditions. Higher order stoichiometries were also observed with 444.20 Da increments.

Table 2. Summary of ligand effects on NC-hairpin complexes

Ligand	NC•SL2	NC•SL3	NC•SL4
Neomycin B	1.9 ± 0.3[a]	31.1 ± 2.8[b]	2.9 ± 0.2[b]
Paromomycin	9.3 ± 1.9[a]	311.1 ± 13.3[b]	17.8 ± 1.2[b]
Tobramycin	10.8 ± 1.7[a]	321.0 ±14.5[b]	17.6 ± 1.3[b]
Ethidium Bromide	13.5 ± 0.6[a]	6.4 ± 0.9[a]	25.5 ± 2.3[a]
Acridine	17.1 ± 0.4[a]	14.5 ± 1.2[a]	46.1 ± 3.4[a]
Mitoxantrone	11.9 ± 1.8[a]	10.3 ± 1.8[a]	6.9 ± 5.9[a]
Daunomycin	44.7 ± 4.0[a]	29.8 ± 1.9[a]	13.1 ± 2.1[a]
Distamycin A	No Effect	58.1 ± 6.3[a]	No Effect
Hoechst 33342	No Effect	No Effect	No Effect
Chlorotetracycline	No Effect	No Effect	No Effect

[a]Dissociation constant (K_d) calculated for ternary NC-hairpin–ligand complexes with 1:1:1 stoichiometry.
[b]Concentration at which 50% of initial NC-hairpin complex was dissociated (IC_{50}) (see Materials and Methods). Values of K_d and IC_{50} are expressed in μM units.

complex with formation of a ternary species. In the case of NC•SL3, for example, the minor groove-binder Hoechst 33342 did not affect the stability of the complex, yielding results identical to those obtained for control samples in the absence of ligand (Figure 7a). Neomycin B induced a concentration-dependent decrease of the NC•SL3 signal and a concomitant increase of the corresponding ligand–SL3 signal, which is consistent with the dissociation of the initial protein–RNA complex (Figure 7b). On the contrary, ternary species were observed for mitoxantrone, which exhibited up to three equivalents bound to the complex and no detectable signs of dissociation (Figure 7c).

A close look at the available high-resolution structures is necessary to rationalize the results of ligand interference. In the NC•SL3 complex, the N-terminal tail of NC folds into a 3_{10} helix that makes contact with the stem's major groove (Figure 8a) (52). Partial obstruction of the upper stem should explain why intercalators and mixed-mode binders provided the same stoichiometries with NC•SL3 as with free SL3, but noticeably lower affinities. Indeed, the binding sites in the upper stem are still accessible from the minor groove side, or during the off-phase of the protein–RNA binding equilibrium, while those in the lower stem remain unhindered by NC. Similarly, a completely unobstructed minor groove enables the binding of the strongest groove-binder, distamycin A, which provided a detectable ternary species.

The ability of aminoglycosides to displace NC and form ligand–SL3 complexes is consistent with at least partially overlapping binding sites on the RNA substrate. In fact, the N-terminal zinc-finger is involved in electrostatic interactions with the major groove of the hairpin upper stem (Figure 8a), which could be alternatively occupied by the aminoglycoside. Further support for competing binding equilibria is provided by the observation that a certain accumulation of drug was necessary in solution before dissociation became apparent. For instance, a 5-fold excess of neomycin B over the initial concentration of NC•SL3 was necessary to obtain ∼30% complex dissociation. An overall IC_{50} of 30.1 ± 2.8 μM was determined for this aminoglycoside (Table 2, see Materials and Methods). It is interesting to note that the other aminoglycosides provided a trend supporting the conclusion that the tightest RNA binder in the series is also the best NC inhibitor.

The complex of NC with SL2 involves interactions between the zinc-fingers and nucleobases exposed on the hairpin tetraloop, in analogy to the SL3 complex (81). In this case, however the 3_{10} helix is packed against the N-terminal knuckle and binds to the minor groove of the AUA platform for further stabilization (Figure 8b). The stem's upper section is still accessible by intercalators and mixed-mode binders from the major groove side, while the lower section is unhindered by

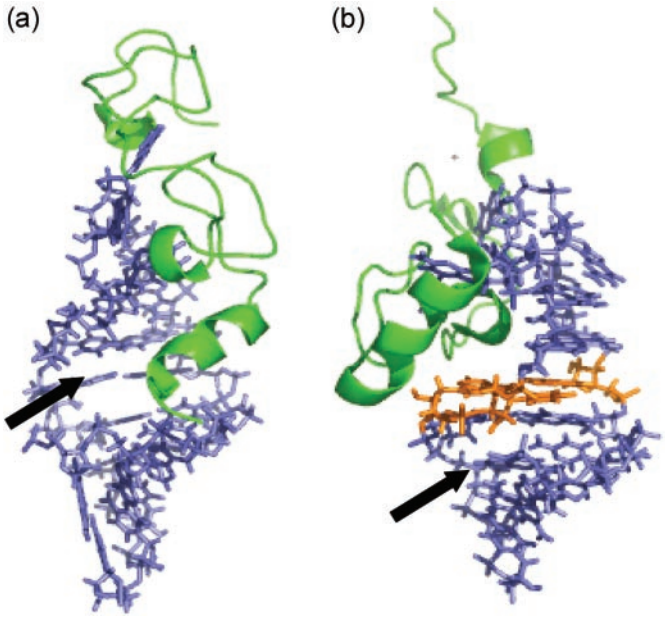

Figure 8. High-resolution structures of (**a**) NC•SL3 (PDB:1A1T) and (**b**) NC•SL2 (PDB:1F6U). The AUA triple base platform is highlighted in orange. The arrows point to the putative binding sites for aminoglycosidic antibiotics.

the protein. For this reason, these ligands were able to bind NC•SL2 with the same stoichiometries observed for free SL2, but weaker overall affinities. The fact that the weak interactions of minor groove-binders were absent in NC•SL2 suggests that these ligands may share a binding site with the protein in the minor groove of the upper stem, which is obstructed by the 3_{10} helix. On the contrary, the presence of a common site is not likely for aminoglycosides, which failed to induce inhibition and instead produced ternary complexes with the same stoichiometries observed for free SL2. These results point towards a possible binding site placed in a relatively wide electronegative area below the triple base platform. This region is located on the major groove side of the stem and is therefore unobstructed by the 3_{10} helix (Figure 8b).

Interpreting the results obtained for NC•SL4 is made more difficult by the absence of a high-resolution structure. Extensive chemical probing of the complex has shown that accessible nucleobases in the loop and tandem wobbles become inert to footprinting agents in the presence of NC, in analogy to the other stem–loops (82). However, it has been suggested that the more compact structure of this tetraloop may be less conducive to protein–RNA interactions, while greater contributions from the upper stem and tandem wobbles are expected to offer stabilization (77,83). In this context, ligand interference can actually provide precious information on the possible spatial arrangement of the NC•SL4 complex. In fact, the inhibitory effects of aminoglycosidic antibiotics indicate a clear competition between ligand and NC for the same region of the RNA structure. As discussed earlier, the putative binding site for aminoglycosides corresponds to a highly electronegative area in the major groove of the tandem wobbles. The same site is certainly capable of effective interactions with the basic N-terminal helix of NC, in agreement with an increased role of the wobbles in stabilizing protein binding. Therefore, all the available information suggests many similarities between the situation of NC•SL4 and NC•SL3, which may still involve weaker contacts of the zinc-fingers with the tetraloop and upper stem, while the 3_{10} helix could reach down to interact with the wobbles in the major groove.

As observed for NC•SL3, the values of IC_{50} for the addition of aminoglycosides to NC•SL4 follow the same trend shown by the K_d's of the correspondent ligand–SL4 complexes (Table 2). In agreement with a competitive binding mechanism, the tightest RNA binder was also found to be the best inhibitor. The much lower IC_{50}'s obtained for NC•SL4 than for NC•SL3 can be explained by a combination of at least two factors. The first is the much weaker affinity of NC for SL4 than for SL3, as shown by K_d values of 1.3 ± 0.5 μM and 178 ± 64 nM for the respective NC complexes (51). The second is the stronger affinity exhibited by the aminoglycosides for free SL4 than for free SL3 (Table 1).

Finally, the lack of effects from minor groove-binders can be attributed to their already weak affinity for free SL4, as well as to possible site overlap. Ideally, minor groove-binders are designed to achieve optimal binding within the deep and narrow groove of B-type DNA (71,72,84). However, in addition to having much wider and shallower dimensions in A-type RNA, the minor groove is further widened in SL4 by the non-canonic pairing of the tandem wobbles. It is conceivable that weak ligand interactions may occur on both the minor and major grooves of this stem–loop, which would explain the observed competition with NC. Considering the behavior of the other NC-hairpin complexes, it was not surprising to obtain ternary species with general intercalators and mixed-mode binders, which provided similar stoichiometries and weaker affinities than with free SL4.

CONCLUSIONS

These results show for the first time that aminoglycosidic antibiotics are capable of disrupting the specific binding of NC to SL3 and SL4 *in vitro*. The role of NC–SL3 interactions in genome recognition and packaging offers the intriguing possibility of employing aminoglycoside analogues to interfere with genome recognition and encapsidation. However, mutagenesis studies have indicated that other 5′-UTR structures contribute to a different extent to the encapsidation process (18,30), thus inhibition of NC–SL3 interactions alone may not completely stop the production of properly packaged virions. The significance of the inhibition of NC–SL4 interactions *in vitro* cannot be evaluated without more information about the role played by the SL4 sequence in stabilizing alternative 5′-UTR conformers through long distance base pairing interactions (40,41). In this direction, future studies will address the hypothesis that the NC-mediated transition between 5′-UTR conformers may involve the binding to a transient hairpin structure, which in this case could provide a favorable target for aminoglycosides activity.

Finally, these results are also emblematic of the many challenges facing the development of small drug ligands to interfere with the interactions of NC with 5′-UTR. The systematic evaluation of archetypical nucleic acid ligands has shown that the ability to bind target RNA stem–loops does not necessarily correlate with actual disruption of NC-hairpin complexes. The range of effects observed for the different ligands is a clear

indication that inhibitory activity is achievable by carefully matching the specific structural features of the target with the characteristics of the ligand. Therefore, greater efforts will be required to identify the most effective target among the many complexes formed by NC with 5′-UTR structures, or to develop broader spectrum ligands capable of simultaneously attacking multiple suboptimal targets.

SUPPLEMENTARY DATA

Supplementary Data are available at NAR Online.

ACKNOWLEDGEMENTS

This research was funded by the National Institutes of Health (R01-GM643208) and the National Science Foundation (CHE-0439067). N.A.H. was also supported by an NIH Chemistry Biology Interface Training Fellowship (T32-GM066706). Funding to pay the Open Access publication charges for this article was provided by National Institutes of Health (R01-GM643208).

Conflict of interest statement. None declared.

REFERENCES

1. Johnson,V.A., Brun-Vezinet,F., Clotet,B., Conway,B., Kuritzkes,D.R., Pillay,D., Shapiro,J.M., Telenti,A. and Richman,D.D. (2005) Update of the drug resistance mutations in HIV-1: 2005. *Top. HIV Med.*, **13**, 51–57.
2. Yusa,K., Kavlick,M.F., Kosalaraksa,P. and Mitsuya,H. (1997) HIV-1 acquires resistance to two classes of antiviral drugs through homologous recombination. *Antivir. Res.*, **36**, 179–189.
3. Schinazi,R.F., Larder,B.A. and Mellors,J.W. (2000) Mutations in retriviral genes associated with drug resistance: 2000-2001 update. *Int. Antivir. News*, **8**, 65–91.
4. Rhee,S.Y., Gonzales,M.J., Kantor,R., Betts,B.J., Ravela,J. and Shafer,R.W. (2003) Human immunodeficiency virus reverse transcriptase and protease sequence database. *Nucleic Acids Res.*, **31**, 298–303.
5. Winters,M.A. and Merigan,T.C. (2005) Insertions in the human immunodeficiency virus type-1 protease and reverse transcriptase genes: clinical impact and molecular mechanisms. *Antimicrob. Agents Chemother.*, **49**, 2575–2582.
6. Chantry,D. (2004) HIV entry and fusion inhibitors. *Expert Opin. Emerg. Drugs*, **9**, 1–7.
7. Winston,A. and Stebbing,J. (2005) New drugs for old. *J. HIV Ther.*, **10**, 11–16.
8. Yu,D., Wild,C.T., Martin,D.E., Morris-Natschke,S.L., Chen,C.H., Allaway,G.P. and Lee,K.H. (2005) The discovery of a class of novel HIV-1 maturation inhibitors and their potential in the therapy of HIV. *Expert Opin. Emerg. Drugs*, **14**, 681–693.
9. Dickson,C., Eisenman,R., Fan,H., Hunter,E. and Reich,N. (1985) In Weiss,R., Teich,N., Varmus,H. and Coffin,J. (eds), *RNA Tumor Viruses*. 2nd ed. Cold Spring Harbor Laboratory Press, Plainview, NY, Vol. 2, pp. 513–648.
10. Darlix,J.L., Lapadat-Tapolsky,M., de Roquigny,H. and Roques,B.P. (1995) First glimpse at structure-function relationships of the nucleocapsid protein of retroviruses. *J. Mol. Biol.*, **254**, 523–537.
11. Lever,A.M., Göttlinger,H.T., Haseltine,W.A. and Sodroski,J.G. (1987) Identification of a sequence required for efficient packaging of human immunodeficiency virus type 1 RNA into virions. *J. Virol.*, **63**, 4085–4087.
12. Linial,M.L. and Miller,A.D. (1990) Retroviral RNA packaging: sequence requirements and implications. *Curr. Top. Microbiol. Immunol.*, **157**, 25–52.
13. Darlix,J.L., Gabus,C., Nugeyre,M.T., Clavel,F. and Barre-Sinussi,F. (1990) Cis elements and trans-acting factors involved in the RNA dimerization of the human immunodeficiency virus HIV-1. *J. Mol. Biol.*, **216**, 689–699.
14. Summers,M.F., Henderson,L.E., Chance,M.R., Bess,J.W.J., South,T.L., Blake,P.R., Sagi,I., Perez-Alvarado,G., Sowder,R.C.I., Hare,D.R. *et al.* (1992) Nucleocapsid zinc fingers detected in retroviruses: EXAFS studies of intact viruses and solution-state structure of the nucleocapsid protein from HIV-1. *Protein Sci.*, **1**, 563–574.
15. Morellet,N., Jullian,N., De Roquigny,H., Maigret,B., Darlix,J.L. and Roques,B.P. (1992) Determination of the structure of the nucleocapsid protein NCp7 from the human immunodeficiency virus type 1 by 1H NMR. *EMBO J.*, **11**, 3059–3065.
16. Rein,A., Henderson,L.E. and Levin,J.G. (1998) Nucleic-acid-chaperone activity of retroviral nucleocapsid proteins: significance for retroviral replication. *Trends Biochem. Sci.*, **23**, 297–301.
17. Clever,J., Sassetti,C. and Parslow,T.G. (1995) RNA secondary structure and binding sites for gag gene products in the 5′ packaging signal of human immunodeficiency virus type 1. *J. Virol.*, **69**, 2101–2109.
18. McBride,M.S. and Panganiban,A.T. (1996) The human immunodeficiency virus type-1 encapsidation site is a multipartite RNA element composed of functional hairpin structures. *J. Virol.*, **70**, 2963–2973.
19. Berkhout,B. (1996) Structure and function of the human immunodeficiency virus leader RNA. *Prog. Nucleic Acids Res. Mol. Biol.*, **54**, 1–34.
20. D'Souza,V. and Summers,M.F. (2005) How retroviruses select their genomes. *Nature Rev. Microbiol.*, **3**, 643–655.
21. Rice,W.G., Shaeffer,C.A., Harten,B., Villinger,F., South,T.L., Summers,M.F., Henderson,L.E., Bess,J.W.,Jr, Arthur,L.O., McDougal,J.S. *et al.* (1993) Inhibition of HIV-1 infectivity by zinc-ejecting aromatic C-nitroso compounds. *Nature*, **361**, 473–475.
22. Rice,W.G., Supko,J.G., Malspeis,L., Buckheit,R.W.,Jr, Clanton,D., Bu,M., Graham,L., Schaeffer,C.A., Turpin,J.A., Domagala,J. *et al.* (1995) Inhibitors of HIV nucleocapsid protein zinc fingers as candidates for the treatment of AIDS. *Science*, **270**, 1194–1197.
23. Miller Jenkins,L.M., Byrd,J.C., Hara,T., Srivastava,P., Mazur,S.J., Stahl,S.J., Inman,J.K., Appella,E., Omichinski,J.G. and Legault,P. (2005) Studies on the mechanism of inactivation of the HIV-1 nucleocapsid protein NCp7 with 2-mercaptobenzamide thioesters. *J. Med. Chem.*, **48**, 2847–2858.
24. Druillennec,S., Dong,C.Z., Escaich,S., Gresh,N., Bousseau,A., Roques,B.P. and Fournie-Zaluski,M.C. (1999) A mimic of HIV-1 nucleocapsid protein impairs reverse transcription and displays antiviral activity. *Proc. Natl Acad. Sci. USA*, **96**, 4886–4891.
25. Pustowka,A., Dietz,J., Ferner,J., Baumann,M., Landersz,M., Konigs,C., Schwalbe,H. and Dietrich,U. (2003) Identification of peptide ligands for target RNA structures derived from the HIV-1 packaging signal psi by screening phage displayed peptide libraries. *Chem. BioChem.*, **4**, 1093–1097.
26. Park,M.Y., Kwon,J., Lee,S., You,J. and Myung,H. (2004) Selection and characterization of peptides specifically binding to HIV-1 psi (Ψ) RNA. *Virus Res.*, **106**, 77–81.
27. Skripkin,E., Paillart,J.C., Marquet,R., Blumenfeld,M., Ehresmann,B. and Ehresmann,C. (1996) Mechanisms of inhibition of *in vitro* dimerization of HIV type I RNA by sense and antisense oligonucleotides. *J. Biol. Chem.*, **271**, 28812–28817.
28. Elmen,J., Zhang,H.-Y., Zuber,B., Ljungberg,K., Wahren,B., Wahlestedt,C. and Liang,Z. (2004) Locked nucleic acid containing antisense oligonucleotides enhance inhibition of HIV-1 genome dimerization and inhibit virus replication. *FEBS Lett.*, **578**, 285–290.
29. Skripkin,E., Paillart,J.C., Marquet,R., Ehresmann,B. and Ehresmann,C. (1994) Identification of the primary site of the human immunodeficiency virus type 1 RNA dimerization *in vitro*. *Proc. Natl Acad. Sci. USA*, **91**, 4945–4949.
30. Paillart,J.C., Shehu-Xhilaga,M., Marquet,R. and Mak,J. (2004) Dimerization of retroviral RNA genomes: an inseparable pair. *Nature Rev. Microbiol.*, **2**, 461–472.
31. Laughrea,M. and Jetté,L. (1994) A 19-nucleotide sequence upstream of the 5′ major splice donor is part of the dimerization domain of human immunodeficiency virus 1 genomic RNA. *Biochemistry*, **33**, 13464–13474.
32. McPike,M.P., Goodisman,J. and Dabrowiak,J.C. (2002) Footprinting and circular dichroism studies on paromomycin binding to the packaging region of human immunodeficiency virus type-1. *Bioorg. Med. Chem.*, **10**, 3663–3672.
33. McPike,M.P., Sullivan,J.M., Goodisman,J. and Dabrowiak,J.C. (2002) Footprinting, circular dichroism and UV melting studies on neomycin B

binding to the packaging region of human immunodeficiency virus type-1 RNA. *Nucleic Acids Res*., **30**, 2825–2831.
34. Ennifar,E., Paillart,J.C., Marquet,R., Ehresmann,B., Ehresmann,C., Dumas,P. and Walter,P. (2003) HIV-1 RNA dimerization initiation site is structurally similar to the ribosomal A site and binds aminoglycoside antibiotics. *J. Biol. Chem*., **278**, 2723–2730.
35. McPike,M.P., Goodisman,J. and Dabrowiak,J.C. (2004) Specificity of neomycin analogues bound to the packaging region of human immunodeficiency virus type 1 RNA. *Bioorg. Med. Chem*., **12**, 1835–1843.
36. Probst,C.L. and Perun,T.J. (1992) *Nucleic acid targeted drug design.* Marcel Dekker, Inc., NY.
37. Hermann,T. (2003) Chemical and functional diversity of small molecule ligands for RNA. *Biopolymers*, **70**, 4–18.
38. Chaires,J.B. (1998) Drug-DNA interactions. *Curr. Opin. Struct. Biol*., **8**, 314–320.
39. Paillart,J.C., Dettenhofer,M., Yu,X.F., Ehresmann,C., Ehresmann,B. and Marquet,R. (2004) First snapshots of the HIV-1 RNA structure in infected cells and in virions. *J. Biol. Chem*., **279**, 48397–48403.
40. Huthoff,H. and Berkhout,B. (2001) Two alternating structures of the HIV-1 leader RNA. *RNA*, **7**, 143–157.
41. Abbink,T.E., Ooms,M., Haasnoot,P.C. and Berkhout,B. (2005) The HIV-1 leader RNA conformational switch regulates RNA dimerization but does not regulate mRNA translation. *Biochemistry*, **44**, 9058–9066.
42. Aleksandrov,M.L., Gall,L.N., Krasnov,V.N., Nikolaev,V.I., Pavlenko,V.A. and Shkurov,V.A. (1984) Extraction of ions from solutions under atmospheric pressure: a method of mass spectrometric analysis of bioorganic compounds. *Dokl. Akad. Nauk*., **277**, 379–383.
43. Yamashita,M. and Fenn,J.B. (1984) Electrospray ion source. Another variation on the free-jet theme. *J. Phys. Chem*., **88**, 4671–4675.
44. Comisarow,M.B. and Marshall,A.G. (1974) Fourier transform ion cyclotron resonance. *Chem. Phys. Lett*., **25**, 282–283.
45. Marshall,A.G., Hendrickson,C.L. and Jackson,G.S. (1998) Fourier transform ion cyclotron resonance mass spectrometry: a primer. *Mass Spectrom. Rev*., **17**, 1–35.
46. Ganem,B., Li,Y.T. and Henion,J.D. (1991) Detection of non-covalent receptor-ligand complexes by mass spectrometry. *J. Am. Chem. Soc*., **113**, 6294–6296.
47. Loo,J.A. (1997) Studying noncovalent protein complexes by electrospray ionization mass spectrometry. *Mass Spectrom. Rev*., **16**, 1–23.
48. Ganguly,A.K., Pramanik,B.N., Tsarbopoulos,A., Covey,T.R., Huang,E. and Fuhrman,S.A. (1992) Mass spectrometric detection of the noncovalent GDP-bound conformational state of the human H-*ras* protein. *J. Am. Chem. Soc*., **114**, 6559–6560.
49. Beck,J.L., Colgrave,M.L., Ralph,S.F. and Sheil,M.M. (2001) Electrospray ionization mass spectrometry of oligonucleotide complexes with drugs, metals, and proteins. *Mass Spectrom. Rev*., **20**, 61–87.
50. Hofstadler,S.A., Sannes-Lowery,K.A. and Hannis,J.C. (2005) Analysis of nucleic acids by FTICR MS. *Mass Spectrom. Rev*., **24**, 265–285.
51. Hagan,N. and Fabris,D. (2003) A direct mass spectrometric determination of the stoichiometry and binding affinity of the complexes between HIV-1 nucleocapsid protein and RNA stem-loops hairpins of the HIV-1 Ψ-recognition element. *Biochemistry*, **42**, 10736–10745.
52. De Guzman,R.N., Wu,Z.R., Stalling,C.C., Pappalardo,L., Borer,P.N. and Summers,M.F. (1998) Structure of the HIV-1 nucleocapsid protein bound to the SL-3 Ψ-RNA recognition element. *Science*, **279**, 384–388.
53. Fabris,D. (2000) Steady-state kinetics of ricin A-chain reaction with the sarcin-ricin loop and with HIV-1 Ψ-RNA hairpins evaluated by direct infusion electrospray ionization mass spectrometry. *J. Am. Chem. Soc*., **122**, 8779–8780.
54. Kim,S.J., Cegelski,L., Studelska,D.R., O'Connor,R.D., Mehta,A.K. and Schaefer,J. (2002) Rotational-echo double resonance characterization of vancomycin binding sites in *Staphylococcus aureus*. *Biochemistry*, **41**, 6967–6977.
55. Jørgensen,T.J.D., Roepstorff,P., Williams,D.H. and Heck,A.J.R. (1998) Determination of solution binding constants for noncovalent complexes between cell wall peptide analogues and vancomycin group antibiotics by electrospray ionzation mass spectrometry. *Anal. Chem*., **70**, 4427–4432.
56. Griffey,R.H., Hofstadler,S.A., Sannes-Lowery,K.A., Ecker,D.J. and Crooke,S.T. (1999) Determinants of aminoglycoside-binding specificity for rRNA by using mass spectrometry. *Proc. Natl Acad. Sci. USA*, **96**, 10129–10133.
57. Maddaford,S.P., Motamed,M., Turner,K.B., Choi,M.S.K., Ramnauth,J., Rakhit,S., Hudgins,R.R., Fabris,D. and Johnson,P.E. (2004) Identification of a novel non-carbohydrate molecule that binds to the ribosomal A-site RNA. *Bioorg. Med. Chem. Lett*., **14**, 5987–5990.
58. Daniel,J.M., Friess,S.D., Rajagopalan,S., Wendt,S. and Zenobi,R. (2002) Quantitative determination of noncovalent binding interactions using soft ionization mass spectrometry. *Int. J. Mass Spectrom. Ion Proc*., **216**, 1–27.
59. Sannes-Lowery,K.A., Griffey,R.H. and Hofstadler,S.A. (2000) Measuring dissociation constants of RNA and aminoglycoside antibiotics by electrospray ionization mass spectrometry. *Anal. Biochem*., **280**, 264–271.
60. Peschke,M., Verkerk,U.H. and Kebarle,P. (2004) Features of the ESI mechanism that affect the observation of multiply charged noncovalent protein complexes and the determination of the association constants by the titration method. *J. Am. Soc. Mass Spectrom*., **15**, 1424–1434.
61. Wan,K.X., Shibue,T. and Gross,M.L. (2000) Non-covalent complexes between DNA-binding drugs and double-stranded oligodeoxynucleotides: a study by ESI ion-trap mass spectrometry. *J. Am. Chem. Soc*., **122**, 300–307.
62. Reyzer,M.L., Brodbelt,J.S., Kerwin,S.M. and Kumar,D. (2001) Evaluation of complexation of metal-mediated DNA-binding drugs to oligonucleotides via electrospray ionization mass spectrometry. *Nucleic Acids Res*., **29**, E103–E103.
63. White,S.A. and Draper,D.E. (1987) Single base bulges in small RNA hairpins enhance ethidium binding and promote allosteric transition. *Nucleic Acids Res*., **15**, 4049–4064.
64. D'Amico,M.L., Paiotta,V., Secco,F. and Venturini,M. (2002) A kinetic study of the intercalation of ethidium bromide into poly(A)•poly(U). *J. Phys. Chem. B*, **106**, 12635–12641.
65. Murray,J.B. and Arnold,J.R.P. (1996) Antibiotic interactions with the hammerhead rybozyme: tetracyclines as a new class of hammerhead inhibitor. *Biochem. J*., **317**, 855–860.
66. Rosenberg,L.S., Carvlin,M.J. and Krugh,T.R. (1986) The antitumor mitoxantrone binds cooperatively to DNA: evidence for heterogeneity in DNA conformation. *Biochemistry*, **25**, 1002–1008.
67. Brown,D.R., Kurz,M., Kearns,D.R. and Hsu,V.L. (1994) Formation of multiple complexes between actinomycin D and a DNA hairpin: structural characterization by multinuclear NMR. *Biochemistry*, **33**, 651–664.
68. Muller,W. and Crothers,D.M. (1968) Studies of the binding of actinomycin and related compounds to DNA. *J. Mol. Biol*., **35**, 251–290.
69. Berman,E., Brown,S.C., James,T.L. and Shafer,R.H. (1985) NMR studies of chromomycin A3 interaction with DNA. *Biochemistry*, **24**, 6887–6893.
70. Fox,K.R. and Howarth,N.R. (1985) Investigations into sequence-selective binding of mithramycin and related ligands to DNA. *Nucleic Acids Res*., **24**, 8695–8714.
71. Spink,N., Brown,D.G., Skelly,J.V. and Neidle,S. (1994) Sequence-dependent effects in drug-DNA interaction: the crystal structure of Hoechst 33258 bound to the $d(CGCAAATTTGCG)_2$ duplex. *Nucleic Acids Res*., **22**, 1607–1612.
72. Tanious,F.A., Ding,D., Patrick,D.A., Bailly,C., Tidwell,R.R. and Wilson,W.D. (2000) Effects of compound structure on carbazole dication-DNA complexes: tests of the minor-groove complex models. *Biochemistry*, **39**, 12091–12101.
73. Gabelica,V., De Pauw,E. and Rosu,F. (1999) Interaction between antitumor drugs and a double-stranded oligonucleotide studied by electrospray ionization mass spectrometry. *J. Mass Spectrom*., **34**, 1328–1337.
74. Fourmy,D., Recht,M.I., Blanchard,S.C. and Puglisi,J.D. (1996) Structure of the A-site of *E.coli* 16S rRNA complexed with an aminoglycoside antibiotic. *Science*, **274**, 1367–1371.
75. Busscher,G.F., Rutjes,F.P.J.T. and van Delft,F.L. (2005) 2-Deoxystreptamine: central scaffold of aminoglycoside antibiotics. *Chem. Rev*., **105**, 775–791.
76. Pappalardo,L., Kerwood,D.J., Pelczer,I. and Borer,P.N. (1998) Three-dimensional folding of an RNA hairpin required for packaging HIV-1. *J. Mol. Biol*., **282**, 801–818.
77. Kerwood,D.J., Cavaluzzi,M.J. and Borer,P.N. (2001) Structure of SL-4 from the HIV-1 packaging signal. *Biochemistry*, **40**, 14518–14529.
78. Amarasinghe,G.K., De Guzman,R.N., Turner,R.B. and Summers,M.F. (2000) NMR structure of stem-loop SL2 of the HIV-1 psi RNA packaging

signal reveals a novel A-U-A base-triple platform. *J. Mol. Biol.*, **299**, 145–156.
79. Turner,K.B., Hagan,N.A. and Fabris,D. (2005) Mapping non-covalent drug binding to HIV-1 Ψ-RNA by tandem mass spectrometry. *Proceedings of the 53rd ASMS Conference on Mass Spectrometry and Allied Topics*, San Antonio, TX .
80. Allain,F.H.-T. and Varani,G. (1995) Divalent metal ion binding to a conserved wobble pair defining the upstream site of cleavage of group I self splicing introns. *Nucleic Acids Res.*, **23**, 341–350.
81. Amarasinghe,G.K., De Guzman,R.N., Turner,R.B., Chancellor,K.J., Wu,Z.R. and Summers,M.F. (2000) NMR structure of the HIV-1 nucleocapsid protein bound to stem-loop SL2 of the Ψ-RNA packaging signal. Implications for genome recognition. *J. Mol. Biol.*, **301**, 491–511.
82. Yu,E. and Fabris,D. (2003) Direct probing of RNA structures and RNA-protein interactions in the HIV-1 packaging signal by chemical modification and electrospray ionization Fourier transform mass spectrometry. *J. Mol. Biol.*, **330**, 211–223.
83. Amarasinghe,G.K., Zhou,J., Miskimon,M., Chancellor,K.J., McDonald,J.A., Matthews,A.G., Miller,R.R., Rouse,M.D. and Summers,M.F. (2001) Stem-loop 4 of the HIV-1 Ψ-RNA packaging signal exhibits weak affinity for the nucleocapsid protein. Structural studies and implications for genome recognition. *J. Mol. Biol.*, **314**, 961–970.
84. Rosu,F., Gabelica,V., Houssier,C. and De Pauw,E. (2002) Determination of affinity, stoichiometry and sequence selectivity of minor groove binder complexes with double-stranded oligodeoxynucleotides by electrospray ionization mass spectrometry. *Nucleic Acids Res.*, **30**, e82.
85. Honig,B. and Nicholls,A. (1995) Classical electrostatics in biology and chemistry. *Science*, **268**, 1144–1149.
86. DeLano,W.L. (2002) *The PyMOL Molecular Graphics System.* DeLano Scientific, San Carlos, CA, USA.